High-Quality Thin Films of UiO-66-NH_2 by Coordination Modulated Layer-by-Layer Liquid Phase Epitaxy

A. Lisa Semrau[a] and Roland A. Fischer*[a]

Abstract: We report the fabrication of macroscopically and microscopically homogeneous, crack-free metal-organic framework (MOF) UiO-66-NH_2 (UiO: Universitetet i Oslo; $[Zr_6O_4(OH)_4(bdc\text{-}NH_2)_6]$; bdc-$NH_2^{2-}$: 2-amino-1,4-benzene dicarboxylate) thin films on silicon oxide surfaces. A DMF-free, low-temperature coordination modulated (CM), layer-by-layer liquid phase epitaxy (LPE) using the controlled secondary building block approach (CSA). Efficient substrate activation was determined as a key factor to obtain dense and smooth coatings by comparing UiO-66-NH_2 thin films grown on ozone and piranha acid-activated substrates. Films of 2.60 μm thickness with a minimal surface roughness of 2 nm and a high sorption capacity of 3.53 mmol g^{-1} MeOH (at 25 °C) were typically obtained in an 80-cycle experiment at mild conditions (70 °C, ambient pressure).

Introduction

Metal-organic frameworks (MOFs) exhibit a porous, crystalline three-dimensional coordination network structure composed of inorganic nodes and multitopic organic linker molecules.[1] Owing to a modular building principle, the chemical and physical properties of the resulting MOFs can be precisely controlled.[2] This allows for various applications ranging from catalysis[3] to photophysical applications[4] and gas separation.[5] The integration of MOFs into devices to exploit their photophysical and electrical properties[6] require crystalline, oriented, and crack-free MOF thin-films on various solid substrates.[7] Such well-defined MOF thin films could also be used to fabricate membranes for gas-phase or liquid phase separations.[8] A research topic garnering increased attention is the fabrication of MOF incorporated membranes for nanofiltration purposes. These can include the filtration of hazardous substances from drinking water[9] or the fabrication of monovalent cation permselective membranes for the extraction of valuable metal cations (e.g., Li^+).[10] In these membranes, UiO-66-NH_2 can either act as a sieve, size or charge selectively separating cations such as Na^+/Mg^{2+} or Li^+/Mg^{2+},[10] or it can be used as a porous addition to a rigid membrane, enhancing the flux while maintaining or enhancing the separation performance of the membrane.[11]

In principle, MOF-based membranes can be fabricated via a mixed membrane approach, where crystalline MOF powder is mixed with a polymer solution to yield a mixed membrane.[12] Another approach is to deposit a MOF thin film on top of a mesoporous substrate.[13] This can be facilitated by either top-down or bottom-up approaches.[14] For the top-down approaches, preformed MOF crystals are spray, spin, or dip-coated onto a surface. For the bottom-up approach, the MOF crystals are assembled by their precursors on top of substrate surfaces. Examples for these processes include the solvothermal deposition/direct synthesis,[15] electrochemical deposition,[16] gas phase-based methods like chemical vapour deposition (CVD) and atomic layer deposition (ALD)[17], and interface dependent methods like Langmuir-Blodgett.[18] One bottom-up method, which is particularly well-known to produce high-quality thin films is layer-by-layer liquid phase epitaxy (LPE).[19] For this stepwise procedure, a support substrate is alternatively treated with a metal-(oxo)-node and an organic linker solution, which are usually dissolved in ethanol. In between these steps, the substrate can be rinsed with ethanol. This procedure is repeated for a defined number of deposition cycles at mild temperatures and ambient pressure yielding a MOF thin film coating on top of the solid support (see Figure 1a). One of the most interesting candidates for the deposition of high-quality MOF thin films is UiO-66 (UiO: Universitetet i Oslo; $[Zr_6O_4(OH)_4(bdc)_6]$; $bdc^{2-} = 1,4$-benzene dicarboxylate). UiO-66 and its analogues (e.g, UiO-66-NH_2, NU-1000) are known for their high chemical[20] and thermal stability[21] and are therefore one of the most investigated MOFs. The first approach to fabricate UiO-66 thin films by LPE was published by our group in 2019.[22] A major challenge that we faced was to modify the high temperature, high-pressure solvothermal synthesis procedures established for microcrystalline UiO-66 powder samples to allow for a low-temperature stepwise approach at ambient pressure. The high temperature during the UiO-66 materials synthesis is usually required to facilitate the self-assembly of the building blocks, where each inorganic node $(Zr_6O_4(OH)_4)^{12+}$ has twelve coordination sites to

[a] A. L. Semrau, Prof. Dr. R. A. Fischer
Department of Chemistry
Inorganic and Metal-Organic Chemistry
Lichtenbergstraße 4, 85787 Garching
E-mail: roland.fischer@tum.de

Supporting information for this article is available on the WWW under https://doi.org/10.1002/chem.202005416

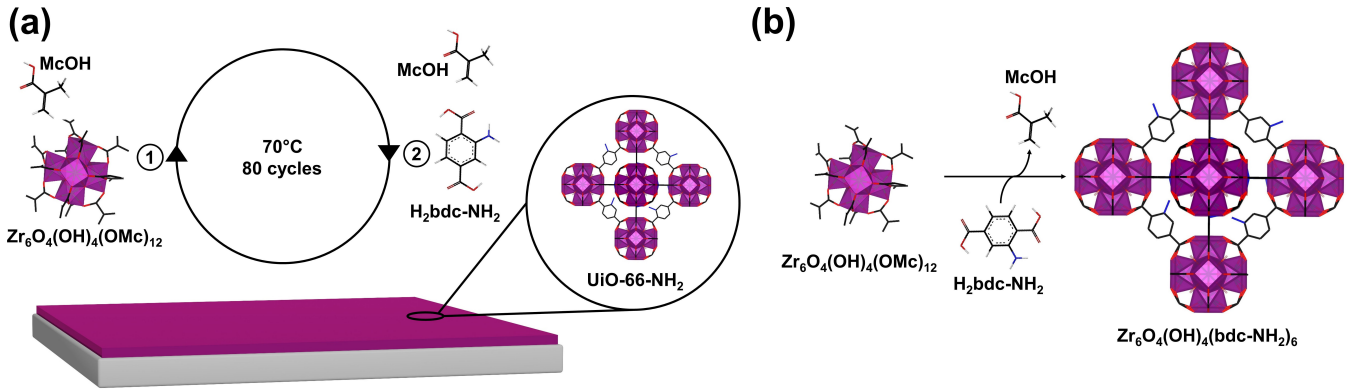

Figure 1. Schematic representation of the CM-LPE deposition (a). A silicon substrate with a native oxide surface is alternately immersed in a $[Zr_6O_4(OH)_4(OMc)_{12}]$/methacrylic acid (McOH) and an H_2bdc-NH_2/methacrylic acid solution forming a UiO-66-NH_2 thin film. (b) Controlled secondary building unit approach, where the framework of UiO-66-NH_2 $[Zr_6O_4(OH)_4$(bdc-$NH_2)_6]$ is formed by the exchange of methacrylate (OMc) ligands with bdc-NH_2 linkers.

bind twelve ditopic linkers (bdc) and building up the 3D framework. The involved substitution kinetics at the Zr sites to form these highly interconnected nodes are complex. To facilitate the associated exchange reactions, we applied the coordination modulation (CM) LPE. The CM method utilizes monocarboxylic acids as additives in solvothermal synthesis. The monocarboxylic acids coordinate to the inorganic nodes and therefore compete with the organic linkers. While this process influences the kinetics as well as the involved coordination equilibria, it makes the synthesis more reproducible. Structural defects such as the deviating coordination modes of organic linkers are more likely to be replaced by modulators, which in turn results in fewer defective structures. Likewise, the CM method was applied for the LPE process, where it has been reported to improve coverage homogeneity and enhance a preferred orientation of the MOF.[23] Another challenge is the formation of the inorganic node $(Zr_6O_4(OH)_4)^{12+}$ during the LPE process. Therefore, instead of employing a metal salt, for example, $ZrCl_4$ or $ZrOCl_2$ as a source for the node the LPE process typically relies on preformed molecular secondary building units (SBUs), for example, $[Zr_6O_4(OH)_4(OMc)_{12}]$ ($^-$OMc = methacrylate). During the deposition, the ligands (e.g., $^-$OMc) are replaced by the organic linkers (bdc^{2-}) to form the MOF. This process is known as the controlled SBU approach (CSA) (see Figure 1b). We applied the CSA-based CM-LPE process to the formation of UiO-66 thin films. After optimizing the conditions, we achieved the fabrication of a nano-crystalline UiO-66 thin film supported on a silicon substrate with a native oxide surface. However, the substrate was not homogeneously covered, but rather an island structure was obtained. Especially for the growth or fabrication of membranes very homogeneous coatings are required. Otherwise, the membranes would contain undesired holes, shortcuts for mass transport, which was pointed out by Xu et al.[10] and Van der Bruggen.[24]

Wöll et al.[25] and others[26] presented another approach to produce thin films of the amine substituted derivative UiO-66-NH_2 ($[Zr_6O_4(OH)_4$(bdc-$NH_2)_6]$; bdc-NH_2 = 2-amino-1,4-benzene dicarboxylate) by LPE utilizing DMF as a solvent and $ZrCl_4$ as a metal source resulting in the formation of crack-free thin films, however with some surface roughness. A comprehensive and comparative overview of the state-of-the-art on UiO-66-NH_2 thin film growth can be found in the Supporting Information, chapter S13.

Due to the need for high-quality thin films of UiO-66 and its linker functionalized analogues, different groups reported the thin film fabrication by various methods, such as solvothermal synthesis,[27] vapour assisted conversion (VAC),[28] electrochemical deposition,[29] and atomic layer deposition.[30] While solvothermal synthesis and electrochemical deposition often lack thickness control and surface homogeneity, atomic layer deposition results in amorphous films, which can be converted to UiO-66 by a post-synthetic treatment. Finally, VAC leads to highly crystalline, homogeneous thin films with a certain degree of thickness control. However, integration of UiO-66 in membrane fabrication based on the VAC thin film deposition process is not possible, due to the VAC mechanism.

Therefore, we decided to further optimize our initial study on CM-LPE of UiO-66 type thin films aiming for more uniform, denser, and crack-free coatings. Herein, we present the fabrication of dense, crystalline, and crack-free UiO-66-NH_2 thin films supported on silicon substrates with native oxide surface by CM-LPE. We used the Zr-oxo methacrylate cluster $[Zr_6O_4(OH)_4(OMc)_{12}]$[31] as a metal source (CSA) and H_2bdc-NH_2 as the linker solution in the environmentally friendly solvent ethanol. As a first step, we optimized the reaction conditions for the UiO-66-NH_2 solvothermal powder synthesis, adapting these parameters in the second step towards the thin film fabrication by CM-LPE. The resulting powder and thin-film samples were investigated by powder X-ray diffraction (PXRD), IR spectroscopy (IR), and scanning electron microscopy (SEM).

Results and Discussion

Nanocrystalline UiO-66-NH_2 powder samples were synthesized prior to thin film deposition via a mild solvothermal solution approach to determine a suitable coordination modulator concentration window for the thin-film growth. For the CSA

approach, the components $[Zr_6O_4(OH)_4(OMc)_{12}]$ and the organic linker (H_2bdc-NH_2) were dissolved in ethanol, and various amounts (0-500 molar equivalents) of the monocarboxylic acid methacrylic acid (McOH) were added as the modulator. The resulting powders were investigated by PXRD, N_2 adsorption experiments, and IR spectroscopy (see Figure 2). The X-ray powder diffractograms show that the most intense reflections at 7.38° and 8.52°, corresponding to the (111) and (200) lattice planes, are present in the samples that were synthesized with 325–500 molar equivalents of methacrylic acid, confirming that the synthesis yielded nano-crystalline UiO-66-NH_2 powders, with crystalline domain sizes of 11 nm (for 500 equiv., calculated by Scherrer equation, see Supporting Information chapter S2).

The IR spectra (Figure 2b) of the powder samples show that the peaks between 1200 and 1660 cm^{-1} sharpen upon the addition of methacrylic acid to the reaction mixture. These vibrations originate from the asymmetric and symmetric stretching of the carboxylic acid and C=C bonds. The C=O peaks correspond to the coordination mode from the carboxylate linker to the Zr-oxo node.[32] For low amounts of modulator the coordination mode of the carboxylate at the Zr node not well defined and shifts to a predominately bridging coordination mode at higher concentrations of the modulator, as displayed by the sharpening of the peaks in the IR spectra. Enlarged images of the corresponding areas can be found in the Supporting Information, chapter S3.

Analysing the N_2 adsorption isotherms of the UiO-66-NH_2 powder samples reveals that the isotherms' shape as well as the BET surface area changes with increasing modulator concentration. Samples with low modulator concentrations (0–100 equiv.) exhibit a type II or type IV isotype. This corresponds to non-porous/macroporous or mesoporous samples, respectively. Samples that were synthesized with higher modulator concentrations (>300 equiv.) feature a typical type I isotherm with minor contributions from a type II isotherm, which confirms the microporosity of the powder samples. The calculated pore size distributions (PSDs, see Supporting Information, chapter S4) depict the same trend as deduced from inspection of the isotherms. Samples obtained with low modulator concentrations are characterized by macro- and mesopores, samples obtained with a high modulator concentration are microporous with minor contributions from macropores. Accordingly, larger (equivalent) BET surface areas were calculated for samples with higher modulator concentrations. The highest BET surface area (949.9 ± 1.8 m^2/g) within the series of samples was observed by adding 500 equiv. of McOH to the reaction. This value is in line with the intermediate range of surface areas reported for UiO-66-NH_2 reference samples obtained by high temperature and high-pressure solvothermal synthesis, which range from 675 m^2/g over 960 m^2/g to 1286 m^2/g.[33]

The evaluation of the IR spectra, PXRD data, and nitrogen adsorption isotherms showed that the addition of 325–500 equiv. of methacrylic acid to the solution yielded nano-crystalline powders with a decreasing amount of meso- and macropores. Due to many reports addressing defect engineering, where modulators are employed strategically to increase the defect concentration,[34] a decreasing amount of macro and mesopores with an increasing amount of modulator may seem counterintuitive at first glance.

However, the crystallization of amorphous MOFs with a molecular SBU as a metal source is very rapid and therefore requires larger amounts of the modulator. We conclude that 325–500 equiv. of methacrylic acid as a modulator represents a suitable parameter window for CM-LPE experiments. It is worth noting that the quality of powder samples and thin films synthesized with the same amount of modulator cannot be compared directly as the fabrication procedures differ significantly.

In the following step, we applied these parameters to the thin film fabrication. The addition of 400 and 500 equiv. of methacrylic acid to the ethanol solutions of the growth components $[Zr_6O_4(OH)_4(OMc)_{12}]$ and H_2bdc-NH_2 did not yield

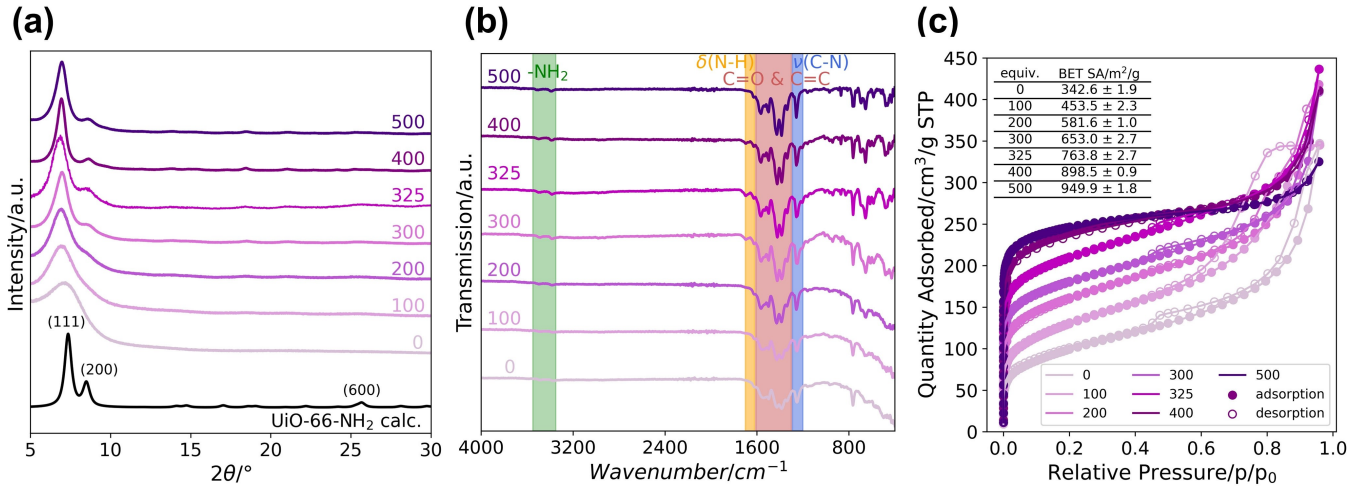

Figure 2. Powder diffractograms (a), IR spectra (b), and N_2 adsorption (c) of dried UiO-66-NH_2 powders synthesized with 0–500 eq. of methacrylic acid as a modulator. The calculated powder pattern was simulated from the single crystal structure of UiO-66-NH_2 (CCDC 1405751, FWHM(2θ) = 0.5) with Vesta.

UiO-66-NH_2 thin film coatings on the SiO_2 substrates. This can be traced back to the etching effect of high modulator concentrations in the solutions. In the next step, we stepwise reduced the excess of the modulator and finally applied 325 equiv. of methacrylic acid to both solutions resulting in a macroscopically homogeneous thin film coating. The grazing incidence powder X-ray diffraction (GIXRD, see Figure 3a) pattern and IR spectrum (Figure 3b) confirms by comparison with the calculated structure and the reference powder samples the successful deposition of a phase-pure, homogenous nanocrystalline UiO-66-NH_2 thin film, with a mean crystallite domain size of 14.7 ± 2 nm. Additionally, we measured the mass-specific methanol (MeOH) adsorption isotherm of the fabricated UiO-66-NH_2 film with a quartz crystal microbalance (QCM). The overall MeOH adsorption capacity is 3.53 mmol g^{-1} MeOH (at 25 °C, 95% MeOH; Figure 3c) and the shape of the isotherm matches a microporous type I isotherm. The small deviation of the adsorption and desorption branch can be attributed to a slow desorption process: The comparison of the mass-specific uptake of methanol with other values reported in literature is difficult, as no methanol adsorption isotherms for UiO-66-NH_2 thin films have been reported to date. However, the ethanol adsorption isotherm of a UiO-66-NH_2 thin film fabricated via the VAC method has been reported.[28] The specific mass uptake of ethanol was determined with a QCM of 2.9 mmol g^{-1}(at 25 °C, 99% EtOH). The 22% higher uptake of methanol reported in this work, in comparison to ethanol, is expected as the size of the molecule increases from methanol to ethanol, likely to reduce the MOF sorption capacity. For UiO-66 powders, the methanol uptake was determined by QCM measurements. These powders adsorb 3.6 mmol g^{-1}, which is very close to the 3.53 mmol g^{-1} MeOH measured in this work.[22] Additionally, we calculated an estimate of 18.8 mmol g^{-1} for the theoretical MeOH uptake of UiO-66-NH_2 when all pores are accessible (see Supporting Information, chapter S5). However, this is discarding all interactions between molecules or the molecules and the framework and models methanol as a simple sphere. Due to these assumptions, the actual maximum theoretical loading is probably significantly lower, in line with the obtained experimental data.

Another important factor is related to the SiO_2 surface activation procedure. Most comments stated, that the cracks in the thin films are a major challenge for any applications.[13] A key to achieving excellent thin-film quality is the careful and efficient activation of the chosen substrate to remove any impurities and to have the maximum amount of nucleation active, functional groups for the MOF thin film formation. We now emphasize optimizing the substrate pre-treatment. Several activation methods were tested. In particular, ozone activation[35] and treatment with piranha acid[36] for 30 min each were utilized, and subsequently, the UiO-66-NH_2 film was deposited via CM-LPE for either 20 or 80 deposition cycles (L). Scanning electron microscopy (SEM; see Figure 4a) revealed that piranha acid activation of SiO_2 surfaces results inhomogeneous, smooth UiO-66-NH_2 coatings. This is attributed to better chemisorption of the components at the substrate surface resulting in higher nucleation density which is assigned to the presence of more hydroxyl groups at the surface created by the piranha etching as compared to ozone treatment. Contact angle measurements of freshly activated SiO_2 surfaces reveal 20° for ozone and 10° for piranha acid treatment (see Supporting Information, chapter S6) and the data support the reasoning.

Additionally, piranha etching is known to also remove organic residues from the surface,[37] creating a cleaner and thus more hydrophilic substrate, which in turn leads to more efficient nucleation for MOF growth. The surface roughness and homogeneity improve for both activation procedures with an increasing number (L) of deposition cycles. The SEM cross-section analysis (Figure 4b) revealed a thickness of 2.60 μm for 80 L, which can be easily adjusted by the number of cycles. The growth of a 20 L UiO-66-NH_2 film resulted in a thickness of 210 nm and 40 L yielded 530 nm. Since the nucleation and crystallite growth kinetics are different the thickness of the thin films increases not strictly linearly as expected for an ideal self-terminated layer by layer growth mechanism.[22] The 80 L

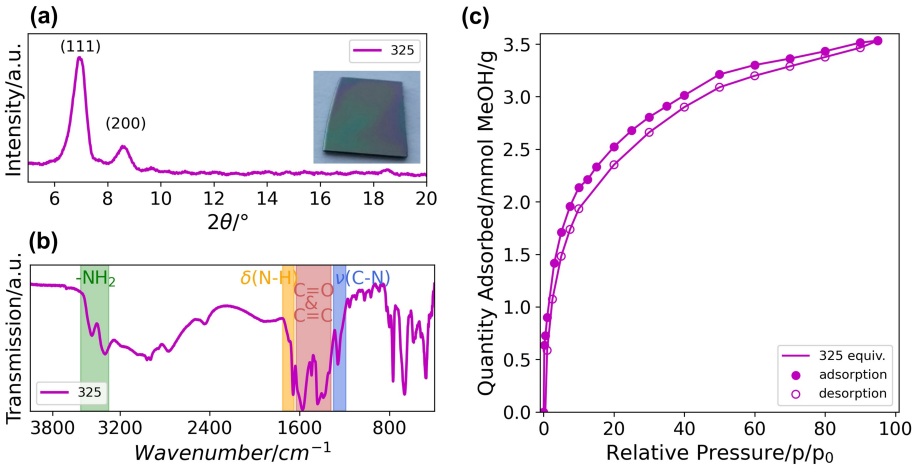

Figure 3. UiO-66-NH_2 thin film (80 L) obtained by CM-LPE with 325 equiv. of methacrylic acid (pink bar) deposited on a SiO_2 surface. GIXRD patterns (a), IR spectrum (b), and methanol adsorption measurement (c).

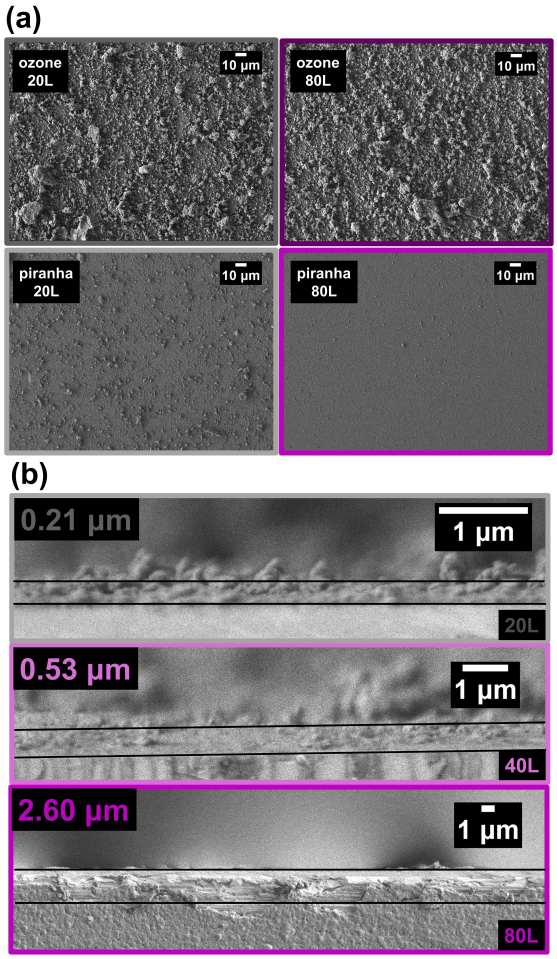

Figure 4. SEM imaging of UiO-66-NH_2 thin films obtained by CM-LPE with 325 equiv. of methacrylic acid supported on a SiO_2 surface which was activated with ozone (dark shade) or piranha acid (light shade) prior to the deposition. (a) Top view of UiO-66-NH_2 thin films after 20 (grey) or 80 (purple) deposition cycles (L). (b) Cross-sections (90°) of the thin films after 20 L (grey), 40 L (light purple), and 80 L (purple).

piranha activated film exhibits a root mean squared roughness of 2.0 nm on a 200×200 nm sample (obtained by Atomic Force Microscopy, AFM). Additional SEM and AFM images for documentation of the film morphology can be found in the Supporting Information, chapter S7 and chapter S8, respectively. Additionally, SEM energy-dispersive X-ray (EDX) elemental mapping was conducted with a UiO-66-NH_2 thin film showing strong peaks at 0.277, 0.392, 0.525, 1.739, and 2.042 keV, assigned to the characteristic X-ray energy of C, N, O, Si, and Zr, respectively (chapter S9). Elemental mapping provided insight into the distribution of the elements within the sample, revealing a uniform elemental distribution. The cross-section analysis enabled a clearer differentiation between the substrate and the UiO-66-NH_2 coating. Overall, we observed a smooth surface without any cracks, which is a significant advancement.

Finally, we investigated the obtained UiO-66-NH_2 thin films by X-ray photoelectron spectroscopy (XPS, Figure 5) to evaluate the defect content, to ensure the correct elemental composition, and to probe for impurities. The XPS survey scan (Figure 5e) revealed an elemental composition of C: 57.3 At%, N: 5.0 At%, O: 32.2 At%, Zr: 5.6 At% with no further impurities. This is in reasonable agreement with the calculated composition of C: 52.1 At%, N: 6.5 At%, O: 34.7 %, Zr: 6.5 At%. As carbon contamination might influence the ratios, comparing N and Zr ratios is more meaningful in this case. The calculated ratio is 1/1 and close to the measured ratio of 1.12/1.0. In literature, deconvoluted XPS spectra were used to determine the relative defect content of UiO-66 thin films.[38] According to Wang et al.,[38] the three different species in the O1s narrow scan can be assigned to the oxygen atoms in free, dangling carboxylic acid groups that do not coordinate to Zr ions, to Zr coordinated carboxylate groups, and to bridging η3-O-Zr_3 groups. As our measurement yielded an O1s peak with no shoulders it is difficult to fit the different components. However, due to this absence of a distinct shoulder, which was observed for other highly defective samples,[38] it can be concluded that the defect content is relatively low. In summary, the XPS results suggest that the synthesis of a relatively low-defect and impurity-free UiO-66-NH_2 thin film was successful. Furthermore, the long-term stability of the 80 L, piranha activated UiO-66-NH_2 thin-film was evaluated in order to verify processability and longevity for manufacturing nanofiltration membranes. Therefore, freshly fabricated thin films were exposed to air for 4 months or immersed in deionized water for 14 days. The stability of the thin films was investigated via GIXRD (see Supporting Information, chapter S10). After the immersion, a slight decrease in the diffraction intensity can be observed over time, which can be attributed to a slow amorphization of the thin film. However, even after 2 weeks of immersing in water, the thin film remains largely crystalline. Usually, membrane long-term stabilities are evaluated by membrane performance tests. Typically, the membranes show a slight decrease in flux and rejection but are overall stable for 70–160 h at elevated pressures up to 16 bar.[40] A comprehensive overview of values reported in literature can be found in the Supporting Information, see chapter S13, Table SI2. Overall, the stability measurements are difficult to compare, nevertheless incorporating this optimized UiO-66-NH_2 thin film into a membrane may significantly increase membrane performance.

Conclusion

Macroscopically and microscopically homogeneous UiO-66-NH_2 thin films were deposited on activated silicon substrates with native oxide surfaces by coordination modulated stepwise liquid phase epitaxy (CM-LPE) following a controlled SBU approach (CSA). The Zr-oxo methacrylate cluster [$Zr_6O_4(OH)_4(OMc)_{12}$] was used as the Zr-oxo node source, H_2bdc-NH_2 as the linker, and methacrylic acid as the modulator in the environmentally friendly solvent ethanol at mild conditions. Efficient substrate activation was determined to be a key factor in obtaining smooth and crack-free UiO-66-NH_2 thin-film coatings. By utilizing piranha acid-activated SiO_2 surfaces UiO-66-NH_2 thin films of uniform coverage, minimal roughness of 2 nm,

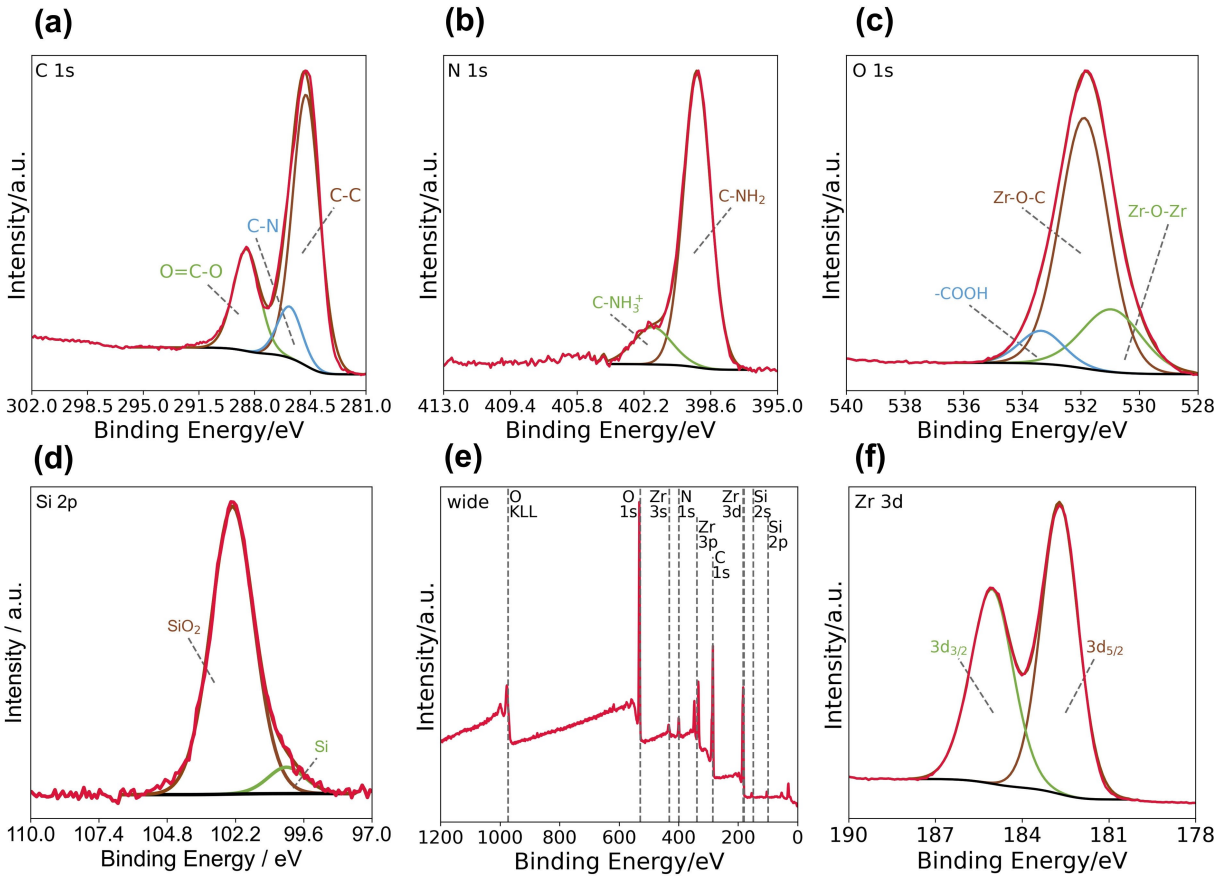

Figure 5. XPS survey scan (e) of a UiO-66-NH_2 thin film as well as narrow scans for 1 s carbon (a), 1 s nitrogen (b) 1 s oxygen (c), 2p silicon (d) and 3d zirconium (e) including assignments to characteristic chemical species.

and a high methanol adsorption capacity of 3.53 mmol g^{-1} were fabricated. The CM-LPE technique allows for precise thickness control via the layer-by-layer technique, which can reproducibly target film thicknesses between 200 nm (20 deposition cycles) and 2.60 μm (80 deposition cycles). Immersed in deionized water the thin films remain crystalline for at least two weeks. Combining the water stability and overall smooth thin film, we suggest using the new CM-LPE protocol for the fabrication of UiO-66-NH_2 based membranes. Additionally, the automatic process and high reproducibility potentially allow for easy upscaling of the membrane fabrication. If the general CM-LPE protocol developed in this work would be adapted to an LBL spray coating process,[40] the upscaling would be further simplified.

Experimental Section

Infrared spectroscopy (IR)

IR measurements are carried out on a Bruker ALPHA-P FTIR in the attenuated total reflectance (ATR) or reflection mode inside an argon-purged glove box. In the case of FTIR ATR, the sample is pressed against a diamond single crystal. Each spectrum consists of 24 accumulated scans with a 2 cm^{-1} resolution.

Powder X-ray diffraction (PXRD)

PXRD measurements of the UiO-66-NH_2 powders are performed on a silicon single-crystal wafer cut in [510] direction using Bragg-Brentano geometry in a PANalytical Empyrean diffractometer equipped with a PANalytical PIXcel 1D detector. Powder patterns of activated samples were recorded on the same instrument in capillary mode. The measurement range is from 5.0° to 50.0° (2θ) with a scan speed of 0.015 degrees per second.

Grazing incidence X-ray diffraction (GIXRD) data were recorded for 2θ angles between 5 and 20° on the same diffractometer with a position-controlled flat sample stage for thin-film measurements. For both modes, X-ray radiation was generated with a Cu tube and K_β radiation is removed by a Ni-filter. Voltage and intensity are 45 kV and 40 mA, respectively. It should be noted that the settings for stability measurements (see Supporting Information, chapter S10) and the measurement in Figure 3 differ significantly as the latter was an overnight measurement and the others were measured for 30 min.

Atomic force microscopy (AFM)

Images are recorded using a Nanosurf easyScan 2 AFM system including a Nanosurf easyScan 2 controller and a Nanosurf isoStage table. A time of 0.6 s per line and 512 points per line is used. Additionally, a setpoint of 70%, a P-Gain of 5000, an I-Gain of 1000, and a D-Gain of 0 is applied. Finally, the free vibration amplitude

equals 59.97 mV. For each sample, the Z-axis orientation is adjusted by cantilever rotation to provide the best resolution. Subsequent image analysis and visualization are performed with the WSxM 5.0 Develop 9.1 software.

Scanning electron microscopy (SEM)

SEM images are obtained with a JEOL JSM-7500F field emission scanning electron microscope with the Gentle Beam mode. EDX spectroscopy was performed with the instrument above and an Oxford Instruments X–Max detector with a 50 mm^2 area. Spectra analysis was conducted with Inca analysis software.

The experimental details for the XPS, N_2 adsorption measurements for the powders, and methanol adsorption experiments for the films can be found in the Supporting Information, chapter S1.

Synthesis Section

In order to optimize the conditions for the fabrication of the UiO-66-NH_2 thin films we initially applied the reaction conditions to the powder synthesis. After optimizing the amount of modulator, we used these conditions for the thin film deposition.

Synthesis of $[Zr_6O_4(OH)_4(OMc)_{12}]$

$[Zr_6O_4(OH)_4(OMc)_{12}]$ was synthesized via a procedure from Kickelbick and Schubert.[31] Therefore, 1 mL 70% w/v $Zr(OPr)_4$ (3.1 mmol) in n-propanol and 1 mL of methacrylic acid (McOH; 11.8 mmol, 5.3 equiv) were mixed at room temperature in a large Schlenk flask under inert conditions. The crystals were collected by filtration after two weeks and washed with small quantities of n-propanol. After drying in vacuo, 860 mg $[Zr_6O_4(OH)_4(OMc)_{12}]$ (0.51 mmol, 98%) could be isolated. The characterization is provided in the Supporting Information (chapter S11).

Synthesis of UiO-66-NH_2 as nanocrystalline powder samples

A sample of 25.5 mg of $[Zr_6O_4(OH)_4(OMc)_{12}]$ (0.015 mmol, 1 equiv.) and x molar equivalents (x = 0–500) of methacrylic acid were dissolved in 4 mL EtOH. A sample of 16.3 mg 4-aminotherephthalic acid (0.09 mmol, 6 equiv.) was dissolved in 12 mL ethanol in a separate vial. Both solutions were separately sonicated for 60 min and mixed afterwards. The reaction mixture was kept at 70 °C for 24 hr. The formed yellow precipitate was washed three times with 4 mL EtOH. In between the washing steps, the precipitate was separated from the solution by centrifugation (7860 rpm, 5 min). Afterwards, the yellow powder is dried at 40 °C in an oven. Characterization data are given and discussed in the main text.

Fabrication of UiO-66-NH_2 thin films by CM-LPE

A double-walled reaction vessel, which was heated with a silicone-oil thermostat and in which the substrate was placed was used for CM-LPE. Peristaltic pumps allowed for reactant filling and washing cycles (computer-controlled by LabView; National Instruments; a picture of the set-up can be found in the Supporting Information, chapter S12). For the thin film deposition, a silicon wafer by Sigert Wafers (100) cut to 1.0×1.0 cm was used as a substrate. Prior to the experiment, the latter were activated in piranha acid at room temperature for 30 min. Subsequently, the substrates were washed with copious amounts of deionized water and ethanol and placed in the double-walled reaction vessel. Afterwards, the silicon substrate was alternatively immersed in ethanol solutions of (A) 1.5 mM $[Zr_6O_4(OH)_4(OMc)_{12}]$ with 488 mM methacrylic acid (325 equiv.) and (B) 9 mM H_2bdc-NH_2 with 488 mM methacrylic acid (325 equiv.). The substrate was kept in every solution at 70 °C for 15 min and the cycle was repeated 80 times.

Stability of UiO-66-NH_2 thin films

For the long-term stability tests, 1×1 cm sized, 80 L, piranha activated UiO-66-NH_2 thin films were exposed to air for 4 months or immersed in 4 mL deionized water for 14 days. The stability of the thin films was investigated via GIXRD (see Supporting Information, chapter S10).

Acknowledgements

A.L.S. is grateful for a PhD scholarship from the Chemical Industry Fund (FCI). This work was supported by the German Research Foundation (DFG) Priority Program 1928 'Coordination Networks: Building Blocks for Functional Systems'. Special thanks to Katja Rodewald for measuring SEM images, Jan Berger for conducting the N_2 adsorption measurements, and Philip M. Stanley for proofreading. We thank Prof. Dr. U. Heiz and Prof. Dr. H. Gasteiger (TU Munich) for allowing us access to the AFM and XPS instruments, respectively. Open access funding enabled and organized by Projekt DEAL.

Conflict of Interest

The authors declare no conflict of interest.

Keywords: CM-LPE · metal-organic frameworks · SURMOFs · thin films · UiO-66-NH_2

[1] a) S. Slomkowski, J. V. Alemán, R. G. Gilbert, M. Hess, K. Horie, R. G. Jones, P. Kubisa, I. Meisel, W. Mormann, S. Penczek, R. F. T. Stepto, *Pure Appl. Chem.* **2011**, *83*, 2229–2259; b) S. Kitagawa, R. Kitaura, S. Noro, *Angew. Chem. Int. Ed.* **2004**, *43*, 2334–2375. *Angew. Chem.* **2004**, *116*, 2388–2430.
[2] a) C. Wang, D. Liu, W. Lin, *J. Am. Chem. Soc.* **2013**, *135*, 13222–13234; b) O. M. Yaghi, M. O'Keeffe, N. W. Ockwig, H. K. Chae, M. Eddaoudi, J. Kim, *Nature* **2003**, *423*, 705–714.
[3] A. Bavykina, N. Kolobov, I. S. Khan, J. A. Bau, A. Ramirez, J. Gascon, *Chem. Rev.* **2020**, *120*, 8468–8535.
[4] a) E. A. Dolgopolova, A. M. Rice, C. R. Martin, N. B. Shustova, *Chem. Soc. Rev.* **2018**, *47*, 4710–4728; b) R. Medishetty, J. K. Zaręba, D. Mayer, M. Samoć, R. A. Fischer, *Chem. Soc. Rev.* **2017**, *46*, 4976–5004.
[5] H. Li, K. Wang, Y. Sun, C. T. Lollar, J. Li, H. C. Zhou, *Mater. Today* **2018**, *21*, 108–121.
[6] I. Stassen, N. Burtch, A. Talin, P. Falcaro, M. Allendorf, R. Ameloot, *Chem. Soc. Rev.* **2017**, *46*, 3185–3241.
[7] J. Liu, C. Wöll, *Chem. Soc. Rev.* **2017**, *46*, 5730–5770.
[8] O. Shekhah, R. Swaidan, Y. Belmabkhout, M. Du Plessis, T. Jacobs, L. J. Barbour, I. Pinnau, M. Eddaoudi, *Chem. Commun.* **2014**, *50*, 2089–2092.
[9] a) Y. He, Y. P. Tang, D. Ma, T. Chung, *J. Membr. Sci.* **2017**, *541*, 262–270; b) M. Golpour, M. Pakizeh, *Chem. Eng. J.* **2018**, *345*, 221–232.
[10] T. Xu, M. A. Shehzad, D. Yu, Q. Li, B. Wu, X. Ren, L. Ge, T. Xu, *ChemSusChem* **2019**, *12*, 2593–2597.
[11] T.-Y. Liu, H. Yuan, Y. Liu, D. Ren, Y. Su, X. Wang, *ACS Nano* **2018**, *12*, 9253–9265.
[12] a) F. Xiao, X. Hu, Y. Chen, Y. Zhang, *ACS Appl. Mater. Interfaces* **2019**, *11*, 47390–47403; b) D. Ma, S. B. Peh, G. Han, S. B. Chen, *ACS Appl. Mater.*

Interfaces **2017**, *9*, 7523–7534; c) L. Liu, X. Xie, S. Qi, R. Li, X. Zhang, X. Song, C. Gao, *J. Membr. Sci.* **2019**, *580*, 101–109.
[13] a) T. Hashem, E. P. Valadez Sánchez, P. G. Weidler, H. Gliemann, M. H. Alkordi, C. Wöll, *ChemistryOpen* **2020**, *9*, 523–523; b) T. Xu, M. A. Shehzad, D. Yu, Q. Li, B. Wu, X. Ren, L. Ge, T. Xu, *ChemSusChem* **2019**, *12*, 2593–2597.
[14] P. Falcaro, R. Ricco, C. M. Doherty, K. Liang, A. J. Hill, M. J. Styles, *Chem. Soc. Rev.* **2014**, *43*, 5513–5560.
[15] D. Zacher, O. Shekhah, C. Wöll, R. A. Fischer, *Chem. Soc. Rev.* **2009**, *38*, 1418–1429.
[16] X. Zhang, K. Wan, P. Subramanian, M. Xu, J. Luo, J. Fransaer, *J. Mater. Chem. A* **2020**, *8*, 7569–7587.
[17] S. Han, C. B. Mullins, *ChemSusChem* **2020**, *13*, 5433–5442.
[18] J. Benito, S. Sorribas, I. Lucas, J. Coronas, I. Gascon, *ACS Appl. Mater. Interfaces* **2016**, *8*, 16486–16492.
[19] O. Shekhah, H. Wang, S. Kowarik, F. Schreiber, M. Paulus, M. Tolan, C. Sternemann, F. Evers, D. Zacher, R. A. Fischer, C. Wöll, *J. Am. Chem. Soc.* **2007**, *129*, 15118–15119.
[20] a) J. E. Mondloch, M. J. Katz, N. Planas, D. Semrouni, L. Gagliardi, J. T. Hupp, O. K. Farha, *Chem. Commun.* **2014**, *50*, 8944–8946; b) J. B. DeCoste, G. W. Peterson, H. Jasuja, T. G. Glover, Y. Huang, K. S. Walton, *J. Mater. Chem. A* **2013**, *1*, 5642.
[21] J. H. Cavka, S. Jakobsen, U. Olsbye, N. Guillou, C. Lamberti, S. Bordiga, K. P. Lillerud, *J. Am. Chem. Soc.* **2008**, *130*, 13850–13851.
[22] A. L. Semrau, S. Wannapaiboon, S. P. Pujari, P. Vervoorts, B. Albada, H. Zuilhof, R. A. Fischer, *Cryst. Growth Des.* **2019**, *19*, 1738–1747.
[23] S. Wannapaiboon, K. Sumida, K. Dilchert, M. Tu, S. Kitagawa, S. Fukukawa, R. Fischer, *J. Adv. Mater. Chem. A* **2017**, *5*, 13665–13673.
[24] F. Aghili, A. A. Ghoreyshi, A. Rahimpour, B. Van der Bruggen, *Ind. Eng. Chem. Res.* **2020**, *59*, 7825–7838.
[25] T. Hashem, E. P. Valadez Sánchez, P. G. Weidler, H. Gliemann, M. H. Alkordi, C. Wöll, *ChemistryOpen* **2020**, *9*, 523–523.
[26] a) D. Ma, G. Han, Z. F. Gao, S. B. Chen, *ACS Appl. Mater. Interfaces* **2019**, *11*, 45290–45300; b) Y. Huang, C. Tao, R. Chen, L. Sheng, J. Wang, *Nanomaterials* **2018**, *8*, 676; c) R. Chen, C. Tao, Z. Zhang, X. Chen, Z. Liu, J. Wang, *ACS Appl. Mater. Interfaces* **2019**, *11*, 43156–43165; d) J. Gao, W. Wei, Y. Yin, M. Liu, C. Zheng, Y. Zhang, P. Deng, *Nanoscale* **2020**, *12*, 6658–6663.
[27] H. Fei, S. Pullen, A. Wagner, S. Ott, S. M. Cohen, *Chem. Commun.* **2015**, *51*, 66–69.
[28] E. Virmani, J. M. Rotter, A. Mähringer, T. von Zons, A. Godt, T. Bein, S. Wuttke, D. D. Medina, *J. Am. Chem. Soc.* **2018**, *140*, 4812–4819.
[29] I. Hod, W. Bury, D. M. Karlin, P. Deria, C.-W. Kung, M. J. Katz, M. So, B. Klahr, D. Jin, Y.-W. Chung, T. W. Odom, O. K. Farha, J. T. Hupp, *Adv. Mater.* **2014**, *26*, 6295–6300.
[30] K. B. Lausund, O. Nilsen, *Nat. Commun.* **2016**, *7*, 13578.
[31] G. Kickelbick, U. Schubert, *Chem. Ber./ Recl.* **1997**, *6*, 473–477.
[32] a) F. Verpoort, T. Haemers, P. Roose, J. P. Maes, *Appl. Spectrosc.* **1999**, *53*, 1528–1534; b) T. Hashem, E. P. Valadez Sánchez, P. G. Weidler, H. Gliemann, M. H. Alkordi, C. Wöll, *ChemistryOpen* **2020**, *9*, 523–523.
[33] a) S.-I. Kim, T.-U. Yoon, M.-B. Kim, S.-J. Lee, Y. K. Hwang, J.-S. Chang, H.-J. Kim, H.-N. Lee, U.-H. Lee, Y.-S. Bae, *Chem. Eng. J.* **2016**, *286*, 467–475; b) A. M. Ploskonka, J. B. DeCoste, *ACS Appl. Mater. Interfaces* **2017**, *9*, 21579–21585; c) D. Azarifar, R. Ghorbani-Vaghei, S. Daliran, A. R. Oveisi, *ChemCatChem* **2017**, *9*, 1992–2000; d) D. T. Lee, J. Zhao, G. W. Peterson, G. N. Parsons, *Chem. Mater.* **2017**, *29*, 4894–4903.
[34] F. Vermoortele, B. Bueken, G. Le Bars, B. Van de Voorde, M. Vandichel, K. Houthoofd, A. Vimont, M. Daturi, M. Waroquier, V. Van Speybroeck, C. Kirschhock, D. E. De Vos, *J. Am. Chem. Soc.* **2013**, *135*, 11465–11468.
[35] J. R. Vig, J. W. Lebus, *IEEE Trans. Parts Hybrids Packag.* **1977**, *12*, 365–370.
[36] K. J. Seu, A. P. Pandey, F. Haque, E. A. Proctor, A. E. Ribbe, J. S. Hovis, *Biophys. J.* **2007**, *92*, 2445–2450.
[37] V. Paredes, E. Salvagni, E. Rodríguez-Castellón, J. M. Manero, *Metall. Mater. Trans. A* **2017**, *48*, 3770–3776.
[38] Y. Wang, L. Li, P. Dai, L. Yan, L. Cao, X. Gu, X. Zhao, *J. Mater. Chem. A* **2017**, *5*, 22372–22379.
[39] a) Y. He, Y. P. Tang, D. Ma, T. Chung, *J. Membr. Sci.* **2017**, *541*, 262–270; b) M. Golpour, M. Pakizeh, *Chem. Eng. J.* **2018**, *345*, 221–232; c) T. Xu, M. A. Shehzad, D. Yu, Q. Li, B. Wu, X. Ren, L. Ge, T. Xu, *ChemSusChem* **2019**, *12*, 2593–2597; d) Y. Gong, S. Gao, Y. Tian, Y. Zhu, W. Fang, Z. Wang, J. Jin, *J. Membr. Sci.* **2020**, *600*, 117874; e) S. Fang, P. Zhang, J. Gong, L. Tang, G. Zeng, B. Song, W. Cao, J. Li, J. Ye, *Chem. Eng. J.* **2020**, *385*, 123400.
[40] H. K. Arslan, O. Shekhah, J. Wohlgemuth, M. Franzreb, R. A. Fischer, C. Wöll, *Adv. Funct. Mater.* **2011**, *21*, 4228–4231.

Manuscript received: December 20, 2020
Accepted manuscript online: April 8, 2021
Version of record online: May 13, 2021

